

Phase retrieval and saddle-point optimization

S. Marchesini^{1,2,*}

¹Lawrence Livermore National Laboratory, 7000 East Ave., Livermore, CA 94550-9234, USA

²Center for Biophotonics Science and Technology, University of California, Davis, 2700 Stockton Blvd., Ste 1400, Sacramento, CA 95817, USA

Iterative algorithms with feedback are amongst the most powerful and versatile optimization methods for phase retrieval. Among these, the hybrid input-output algorithm has demonstrated remarkable success in performing giga-element nonlinear optimization, escaping local minima and producing images at resolutions beyond the capabilities of lens-based optical methods. Here the input-output iteration is improved by a lower dimensional subspace saddle-point optimization.

OCIS codes: 100.5070

Phase retrieval is one of the toughest challenges in optimization, requiring the solution of a large-scale non-linear, non-convex and non-smooth constrained problem. Efficient algorithms are being used in astronomical imaging, electron microscopy, lensless x-ray imaging and x-ray crystallography, substituting lenses and other optical elements in the image-forming process.

Novel experimental methods are being developed thanks to advances in optimization techniques (see e.g.¹ for a review), primarily the introduction of a control-feedback method proposed by Fienup (Hybrid Input Output-HIO^{2,3}). The important theoretical insight that these iterations may be viewed as projections in Hilbert space^{4,5} has allowed theoreticians to analyze and improve on the basic HIO algorithm^{6,7,8,9}.

The algorithm proposed is a reformulation of the HIO algorithm from an unusual perspective. Such algorithm seeks the saddle-point of the difference between data and constraint errors, minimizing this difference when moving within the constraints, and maximizing it when moving outside the constraints¹⁰. Here, ideas from other optimization techniques are utilized to improve upon the original HIO algorithm.

1. Phase retrieval problem

When we record the diffraction pattern intensity of light scattered by an object the phase information is missing. Apart from normalization factors, an object with density $\rho(\mathbf{r})$, \mathbf{r} being the coordinates in the *object* (or *real*) space, generates a diffraction pattern intensity equal to the modulus square of the Fourier Transform (FT) $\tilde{\rho}(\mathbf{k})$:

$$I(\mathbf{k}) = |\tilde{\rho}(\mathbf{k})|^2 \quad (1)$$

Where \mathbf{k} represent the coordinate in the Fourier (or Reciprocal) space. In absence of constraints, any phase $\varphi(\mathbf{k})$

can be applied to form our solution $\tilde{\rho} = \sqrt{I}e^{i\varphi}$. Phase retrieval consists in solving (Eq. 1) from the measured intensity values $I(\mathbf{k})$ and some other prior knowledge (constraints).

Diffraction microscopy solves the phase problem using the knowledge that the object being imaged is isolated, it is assumed to be 0 outside a region called support S :

$$\rho(\mathbf{r}) = 0, \text{ if } \mathbf{r} \notin S \quad (2)$$

A projection onto this set (\mathbf{P}_s) involves setting to 0 the components outside the support, while leaving the rest of the values unchanged (Fig. 1(a)):

$$\mathbf{P}_s \rho(\mathbf{r}) = \begin{cases} \rho(\mathbf{r}) & \text{if } \mathbf{r} \in S \\ 0 & \text{otherwise} \end{cases} \quad (3)$$

and its complementary projector $\mathbf{P}_{\bar{s}} = \mathbf{I} - \mathbf{P}_s$.

The projection to the nearest solution of (Eq. 1) in reciprocal space is obtained by setting the modulus to the measured one $m(\mathbf{k}) = \sqrt{I(\mathbf{k})}$, and leaving the phase unchanged (Fig. 1(b)):

$$\tilde{\mathbf{P}}_m \tilde{\rho}(\mathbf{k}) = \tilde{\mathbf{P}}_m |\tilde{\rho}(\mathbf{k})| e^{i\varphi(\mathbf{k})} = \sqrt{I(\mathbf{k})} e^{i\varphi(\mathbf{k})}, \quad (4)$$

Such projector is a “diagonal” operator in Fourier space, acting element-by-element on each amplitude. When applied to real-space densities $\rho(\mathbf{r})$, it becomes non-local, mixing every element with a forward \mathcal{F} and inverse \mathcal{F}^{-1} Fourier transform:

$$\mathbf{P}_m = \mathcal{F}^{-1} \tilde{\mathbf{P}}_m \mathcal{F}. \quad (5)$$

The Euclidean length $\|\rho\|$ of a vector ρ is defined as:

$$\|\rho\|^2 = \rho^\dagger \cdot \rho = \sum_{\mathbf{r}} |\rho(\mathbf{r})|^2 = \sum_{\mathbf{k}} |\tilde{\rho}(\mathbf{k})|^2. \quad (6)$$

If noise is present, it should be used to weight the sum. The distance from the current point to the corresponding set $\|\mathbf{P}\rho - \rho\|$ is the basis for our error metric:

$$\begin{aligned} \varepsilon_s(\rho) &= \|\mathbf{P}_s \rho - \rho\|, \\ \varepsilon_m(\rho) &= \|\mathbf{P}_m \rho - \rho\|, \end{aligned} \quad (7)$$

*Current address: Lawrence Berkeley National Laboratory, 1 Cyclotron Rd, Berkeley CA 94720, USA. e-mail: smarchesini@lbl.gov

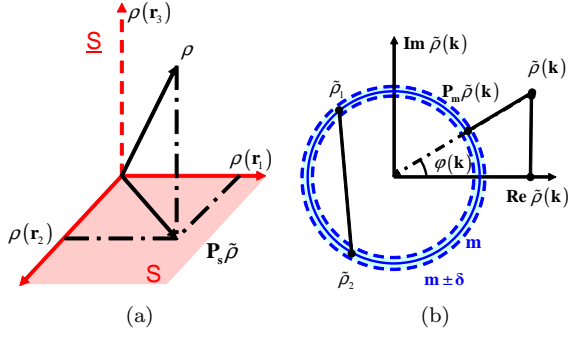


Fig. 1. Examples of sets and projectors: (a) Support: The axes represent the values on 3 pixels of an image ρ known to be 0 outside the support. The vertical axis $\rho(\mathbf{r}_3)$ represents a pixel outside the support ($\mathbf{r}_3 \in \underline{S}$), while the horizontal plane represents pixels inside the support S . The projection on this set is performed simply by setting to 0 all the pixels outside the support. (b) Modulus: A pixel (in Fourier space) with a given complex value is projected on the closest point on the circle defined by the radius m . If there is some uncertainty in the value of the radius $m \pm \delta$, the circle becomes a band. The circle is a non-convex set, since the linear combination between two points on the same set, ρ_1 and ρ_2 does not lie on the set. Also represented in the figure is the projection on the real axis (reality projection).

or their normalized version $\bar{\varepsilon}_{s,m}(\rho) = \frac{\varepsilon_{s,m}(\rho)}{\|\mathbf{P}_{s,m}\rho\|}$.

The gradients of the error metrics can be expressed in terms of projectors:^{3,11}

$$\nabla \varepsilon_m^2(\rho) = -2[\mathbf{P}_m - \mathbf{I}]\rho \quad (8)$$

$$\nabla \varepsilon_s^2(\rho) = -2[\mathbf{P}_s - \mathbf{I}]\rho, \quad (9)$$

Steps of $-\frac{1}{2}\nabla \varepsilon_{s,m}^2$ bring the corresponding error metrics to 0. The solution, hopefully unique, is obtained when both error metrics are 0.

2. minimization in feasible space

One popular algorithm (Gerchberg and Saxton¹³) minimizes the error metric $\varepsilon_m(\rho)$

$$\begin{aligned} \min_{\rho} \varepsilon_m^2(\rho) \\ \text{subject to } \mathbf{P}_{\underline{s}}\rho = 0. \end{aligned} \quad (10)$$

We apply the constraint $\mathbf{P}_{\underline{s}}\rho = 0$ and move only in the feasible space $\rho = \rho_s = \mathbf{P}_s\rho$ and rewrite as:

$$\min_{\rho_s} \varepsilon_m^2(\rho_s) \quad (11)$$

The steepest descent direction is projected onto S :

$$\begin{aligned} \rho^{(n+1)} &= \rho^{(n)} + \Delta\rho^{(n)}, \\ \Delta\rho^{(n)} &= -\frac{1}{2}\nabla_s \varepsilon_m^2(\rho^{(n)}), \\ &= -\mathbf{P}_s[\mathbf{I} - \mathbf{P}_m]\rho, \end{aligned} \quad (12)$$

where $\nabla_s = \mathbf{P}_s\nabla$ is the component of the gradient in the support. Notice that a step of $-\frac{1}{2}\nabla \varepsilon_m^2(\rho)$ brings the error $\varepsilon_m^2(\rho)$ to 0. The projection of this step is shorter than the step itself, and gives a lower bound for the optimal step length. This algorithm is usually written as a projection algorithm:

$$\begin{aligned} \rho^{(n+1)} &= \rho^{(n)} + \Delta\rho^{(n)}, \\ &= \mathbf{P}_s\mathbf{P}_m\rho^{(n)}. \end{aligned} \quad (13)$$

By projecting back and forth between two sets, it converges to the local minimum. Such algorithm is commonly referred to as Error Reduction (ER) in the phase retrieval community.

The simplest acceleration strategy, the steepest descent method, performs a line search of the local minimum in the steepest descent direction:

$$\min_{\delta} \varepsilon_m^2(\rho + \delta\Delta\rho). \quad (14)$$

At a minimum any further movement in the direction of the current step increases the error metric; the gradient direction must be perpendicular to the current step. In other words the current step and the next step become orthogonal:

$$\begin{aligned} \frac{\partial}{\partial \delta} \varepsilon_m^2(\rho + \delta\Delta\rho) &= \langle \Delta\rho | \mathbf{P}_s[\mathbf{I} - \mathbf{P}_m](\rho + \delta\Delta\rho_s) \rangle_r, \\ 0 &= \langle \Delta\rho_s | [\mathbf{I} - \mathbf{P}_m](\rho + \delta\Delta\rho_s) \rangle_r, \end{aligned} \quad (15)$$

where $\langle \mathbf{x} | \mathbf{y} \rangle_r = \Re(\mathbf{x}^\dagger \cdot \mathbf{y})$. The line search algorithm can use ε_m^2 , and/or its derivative in (Eq. 15). This optimization should be performed in reciprocal space, where the modulus projector is fast to compute (Eq. (4)), while the support projection requires two Fourier transforms:

$$\tilde{\mathbf{P}}_s = \mathcal{F}\mathbf{P}_s\mathcal{F}^{-1}, \quad (16)$$

but it needs to be computed once to calculate $\Delta\rho_s$.

The steepest descent method is known to be inefficient in the presence of long narrow valleys, where imposing that successive steps be perpendicular causes the algorithm to zig-zag down the valley. This problem is solved by the non-linear conjugate gradient method^{14,15,16,17,18}.

3. Saddle-point optimization

The following algorithm is a reformulation of the HIO algorithm from a gradient/constraint perspective. We seek the saddle point of the error-metric difference $\mathcal{L}(\rho) = \varepsilon_m^2(\rho) - \varepsilon_s^2(\rho)$ ¹⁰:

$$\min_{\rho_s} \max_{\rho_{\underline{s}}} \mathcal{L}(\rho_s + \rho_{\underline{s}}). \quad (17)$$

using equations (8) and (9) we obtain the gradient:

$$\nabla \mathcal{L}(\rho) = 2[\mathbf{P}_s - \mathbf{P}_m]\rho. \quad (18)$$

Since we seek the saddle point, the step direction has to go in the descent direction for ρ_s ($-\mathbf{P}_s\nabla$) and ascent

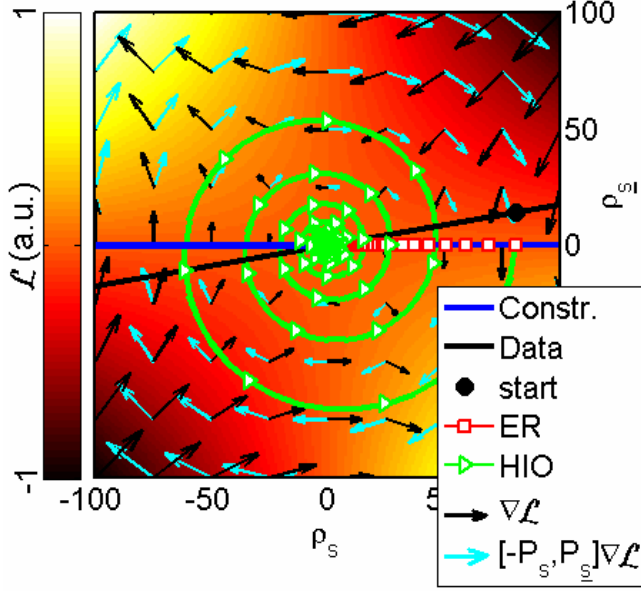


Fig. 2. Algorithms seek the intersection between two sets (data and constraints) in different ways: ER projects back and forth between the two sets. HIO seeks the saddle point of the difference of the distances (ε^2) between the current point and the two sets ($\mathcal{L} = \varepsilon_m^2 - \varepsilon_s^2$), represented in background in pseudocolormap. The gradient ($\nabla \mathcal{L}$) is indicated by black arrows; by inverting the direction parallel to the constraint ($-\mathbf{P}_s$, left-right, depicted by azure arrows) HIO moves in a descent-ascent direction ($[-\mathbf{P}_s + \mathbf{P}_s] \nabla \mathcal{L}$) spiraling toward the $\min_s \max_s$ saddle point.

direction ($+\mathbf{P}_s \nabla$) for ρ_s . For reasons discussed below, we reduce the \mathbf{P}_s component by a factor $0.5 \leq \beta \leq 1$:

$$\begin{aligned} \Delta \rho &= \{-\mathbf{P}_s + \bar{\beta} \mathbf{P}_s\} \frac{1}{2} \nabla \mathcal{L}(\rho), \\ &= \{\mathbf{P}_s[\mathbf{P}_m - \mathbf{P}_s] - \bar{\beta} \mathbf{P}_s[\mathbf{P}_m - \mathbf{P}_s]\} \rho, \\ &= \{\mathbf{P}_s[\mathbf{P}_m - \mathbf{I}] - \bar{\beta} \mathbf{P}_s \mathbf{P}_m\} \rho. \end{aligned} \quad (19)$$

The new iteration point:

$$\begin{aligned} \rho^{(n+1)} &= \rho^{(n)} + \Delta \rho^{(n)} \\ &= [\mathbf{P}_s \mathbf{P}_m - \bar{\beta} \mathbf{P}_s[\mathbf{I} - \mathbf{P}_m]] \rho^{(n)} \end{aligned} \quad (20)$$

can be expressed in a more familiar form of the HIO algorithm^{2,3}:

$$\rho^{(n+1)}(\mathbf{r}) = \begin{cases} \mathbf{P}_m \rho^{(n)}(\mathbf{r}) & \text{if } \mathbf{r} \in S, \\ (\mathbf{I} - \bar{\beta} \mathbf{P}_m) \rho^{(n)}(\mathbf{r}) & \text{otherwise.} \end{cases} \quad (21)$$

Rather than setting to 0 the object $\rho(\mathbf{r})$ where it is known to be 0 ($\mathbf{r} \notin S$), the feedback term seeks a stable condition of a loop system, decreasing the rate of change in the object density produced by the nonlinear operator \mathbf{P}_m .

Optimization of the step length is obtained by increasing a multiplication factor δ until the current and next

search directions become perpendicular to one another:

$$\langle \Delta \rho | [-\mathbf{P}_s + \bar{\beta} \mathbf{P}_s] \nabla \mathcal{L}(\rho + \delta \Delta \rho) \rangle_r = 0. \quad (22)$$

A more robust strategy involves replacing the one dimensional search with a two dimensional optimization of the saddle point:

$$\begin{aligned} &\min_{\alpha} \max_{\beta} \psi(\alpha, \beta), \\ \psi(\alpha, \beta) &= \mathcal{L}(\rho + \alpha \Delta \rho_s + \beta \Delta \rho_s). \end{aligned} \quad (23)$$

where both components ($\mathbf{P}_s, \mathbf{P}_s$) of successive steps are perpendicular to one another:

$$\begin{aligned} \frac{\partial \psi}{\partial \alpha} &= \langle \Delta \rho_s | \nabla \mathcal{L}(\rho + \alpha \Delta \rho_s + \beta \Delta \rho_s) \rangle_r = 0, \\ \frac{\partial \psi}{\partial \beta} &= \langle \Delta \rho_s | \nabla \mathcal{L}(\rho + \alpha \Delta \rho_s + \beta \Delta \rho_s) \rangle_r = 0. \end{aligned} \quad (24)$$

This two dimensional minmax problem needs to be fast to provide real acceleration and will be discussed in the following section.

A. Discussion

The large dimensional minmax problem (Eq. 17) can be expressed in a dual form:

$$\begin{cases} \min_{\rho_s} \varepsilon_m^2(\rho) = \min_{\rho_s} \|\mathbf{I} - \mathbf{P}_m\| \rho^2 \\ \min_{\rho_s} \varepsilon_s^2(\rho) - \varepsilon_m^2(\rho) = \min_{\rho_s} 2 \langle \mathbf{P}_m \rho | \rho \rangle_r + c \end{cases} \quad (25)$$

The upper optimization is similar to the problem treated in Section 2, converging to a local minimum with a simple projected gradient method. The lower function, however, can be discontinuous in the presence of zeros ($\tilde{\rho}_s = 0$) in Fourier space:

$$\langle \tilde{\mathbf{P}}_m \tilde{\rho} | \tilde{\rho} \rangle = \sum \sqrt{I} |\tilde{\rho}_s + \tilde{\rho}_s| \quad (26)$$

which is a non-smooth v-shaped function of $\tilde{\rho}_s$ for $\tilde{\rho}_s = 0, \sqrt{I} > 0$, and simple gradient methods oscillate around minima. The projected gradient step can be overestimated and requires the relaxation parameter $\bar{\beta}$. Zeros in Fourier space are candidates (necessary but not sufficient condition) for the location of phase vortices, phase discontinuities, which are known to cause stagnation²⁰. Analytical²³, statistical^{20,21,22}, and deterministic^{24,25} methods have been proposed to overcome such singularities.

4. Two dimensional subproblem

The local saddle point (Eq. 23) requires two conditions to be met. The first order condition is that the solution is a stationary point, where the gradient of ψ is 0 (Eq. 24):

$$\begin{aligned} \nabla_{\tau} \psi(\tau) &= \langle \Delta \rho | \nabla_{\rho} \mathcal{L}(\rho + \tau^T \Delta \rho) \rangle_r = 0, \\ \tau &= \begin{pmatrix} \alpha \\ \beta \end{pmatrix}, \Delta \rho = \begin{pmatrix} \Delta \rho_s \\ \Delta \rho_s \end{pmatrix}, \nabla_{\rho} = \begin{pmatrix} \nabla_s \\ \nabla_s \end{pmatrix}. \end{aligned} \quad (27)$$

This ensures that both components $(\mathbf{P}_s, \mathbf{P}_{\bar{s}})$ of successive steps $\Delta\rho^{(n)}, \Delta\rho^{(n+1)}$ are perpendicular. Notice that $\frac{1}{2}\nabla_{\boldsymbol{\tau}}\psi(0) = \begin{pmatrix} -\|\Delta\rho_s\|^2 \\ +\|\Delta\rho_{\bar{s}}\|^2 \end{pmatrix}$.

The second order conditions (min-max) require the Hessian \mathcal{H} of ψ (the Jacobian of (Eq. 27)) to be symmetric and indefinite (neither positive nor negative definite):

$$\mathcal{H}_{\boldsymbol{\tau}} = \begin{pmatrix} \partial_{\alpha}\partial_{\alpha} & \partial_{\alpha}\partial_{\beta} \\ \partial_{\beta}\partial_{\alpha} & \partial_{\beta}\partial_{\beta} \end{pmatrix} \psi, \begin{cases} \mathcal{H}_{\alpha,\alpha} \geq 0, \\ \mathcal{H}_{\beta,\beta} \leq 0. \end{cases} \quad (28)$$

This Hessian is computed analytically in appendix, it is small (2×2), and can be used to compute the Newton step:

$$\Delta\boldsymbol{\tau} = -\mathcal{H}^{-1}\nabla_{\boldsymbol{\tau}}\psi. \quad (29)$$

However, the Hessian precise value is not necessary and requires an effort that could be avoided by other methods.

The minimal residual method optimizes the norm of the gradient:

$$\min_{\boldsymbol{\tau}} \Phi(\boldsymbol{\tau}), \quad \Phi = \frac{1}{2} \|\nabla_{\boldsymbol{\tau}}\psi(\boldsymbol{\tau})\|^2, \quad (30)$$

transforming the saddle point problem in a minimization problem, and providing the metric Φ to monitor progress. However by minimizing the norm of the gradients, we can move to other stationary points and the algorithm becomes less robust.

The HIO algorithm uses a good guess for the Hessian, which is often all it is needed to achieve fast convergence:

$$\Delta\boldsymbol{\tau} = -\hat{\mathcal{H}}^{-1}\nabla_{\boldsymbol{\tau}}\psi(\boldsymbol{\tau}), \quad (31)$$

$$\hat{\mathcal{H}} = 2 \begin{pmatrix} 1 & 0 \\ 0 & -1/\beta \end{pmatrix} (\Delta\rho\Delta\rho^T), \quad (32)$$

$$\boldsymbol{\tau}^{(n+1)} = \boldsymbol{\tau}^{(n)} + \Delta\boldsymbol{\tau}^{(n)}. \quad (33)$$

Starting from $\boldsymbol{\tau}^{(0)} = \mathbf{0}$, the first iteration gives the standard HIO step $\boldsymbol{\tau}^{(1)} = \begin{pmatrix} 1 \\ \beta \end{pmatrix}$. The Hessian \mathcal{H} satisfies condition (Eq. 28), ensuring that $\Delta\boldsymbol{\tau}$ is less then 90° from the direction of the saddle. We can perform a line search using the preconditioner $\hat{\mathcal{H}}^{-1}$:

$$\left\langle \Delta\boldsymbol{\tau} | \hat{\mathcal{H}}^{-1} \nabla_{\boldsymbol{\tau}}\psi(\boldsymbol{\tau} + \delta\Delta\boldsymbol{\tau}) \right\rangle_r = 0. \quad (34)$$

However the Hessian of $\hat{\mathcal{H}}^{-1}\psi$ is antisymmetric, the algorithm is unstable and could spiral away from the solution. The bi-conjugate gradient method applies to symmetric indefinite Hessians and monitors progress of the algorithm. Conjugate directions $\Lambda\boldsymbol{\tau}$ replace the steepest descent direction in the line search:

$$\begin{aligned} \Lambda\boldsymbol{\tau}^{(n+1)} &= \Delta\boldsymbol{\tau}^{(n+1)} + \gamma^{(n)}\Lambda\boldsymbol{\tau}^{(n)} \\ \gamma^{(n)} &= \frac{\langle \Delta\boldsymbol{\tau}^{(n+1)} | \hat{\mathcal{H}}^{(-1)} (\nabla\psi(\boldsymbol{\tau}^{(n+1)}) - \nabla\psi(\boldsymbol{\tau}^{(n)})) \rangle}{\langle \Delta\boldsymbol{\tau}^{(n)} | \hat{\mathcal{H}}^{-1} \Delta\nabla\psi(\boldsymbol{\tau}^{(n)}) \rangle} \end{aligned} \quad (35)$$

A better option is to use a quasi-Newton method, by updating the Hessian based on the new gradient values.

The *Symmetric Rank 1* method can be applied to indefinite problems¹⁹:

$$\begin{aligned} \mathbf{y} &= \nabla_{\boldsymbol{\tau}}\psi(\boldsymbol{\tau} + \Delta\boldsymbol{\tau}) - \nabla_{\boldsymbol{\tau}}\psi(\boldsymbol{\tau}) \\ \Delta\mathcal{H}^{-1} &= \frac{\|\Delta\boldsymbol{\tau} - \mathcal{H}^{-1}\mathbf{y}\|^2}{(\Delta\boldsymbol{\tau} - \mathcal{H}^{-1}\mathbf{y})^T \cdot \mathbf{y}} \\ \mathcal{H}^{-1} &\rightarrow \mathcal{H}^{-1} + \Delta\mathcal{H}^{-1} \end{aligned} \quad (36)$$

Second order conditions (Eq. 28) can be imposed to the Hessian, by flipping the sign or setting to 0 the values that violate them. Φ can be used to monitor progress, as long as we are in the neighborhood of the solution and the Hessian satisfies second order conditions (Eq. 28). It was found that the Hessian and step size parameters were fairly constant for each 2D optimization, therefore the first guess for $\boldsymbol{\tau}$ and \mathcal{H} was obtained from the average of the previous 5 of such optimizations.

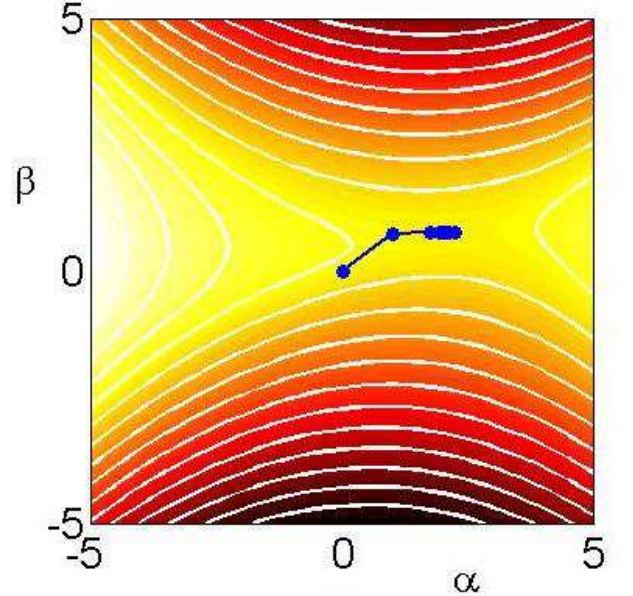


Fig. 3. pseudocolor- and contourmap of $\psi(\alpha, \beta)$ are depicted in the background. Iterations to the 2D saddle point are shown in blue.

In summary, an efficient algorithm is obtained by a combination of HIO/quasi-Newton/Newton methods with a trust region $|\Delta\boldsymbol{\tau}| \leq r$:

1. calculate step $\Delta\rho = -\frac{1}{2} \begin{pmatrix} \nabla_s \mathcal{L} \\ -\nabla_{\bar{s}} \mathcal{L} \end{pmatrix}$, and set trust region radius $r = r_{\max}$.
2. if the iteration number is ≤ 5 , use HIO as first guess: $\mathcal{H} = \hat{\mathcal{H}}, \boldsymbol{\tau} = (1, \beta)$.
3. otherwise average 5 previous optimized step sizes $\boldsymbol{\tau}$, and Hessians \mathcal{H} , and use the average as initial guess.
4. calculate gradient $\nabla\psi(\boldsymbol{\tau})$. If small, exit loop (go to 10).

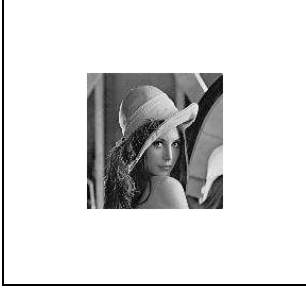


Fig. 4. Test figure used for benchmarking (total size: 256^2 , object size: 128^2 pixels).

5. compute Newton step using approximate Hessian:
 $\Delta\tau = -\mathcal{H}^{-1}\nabla\psi$, enforce trust region $|\Delta\tau| < r$.
6. update Hessian with SR1 method (Eq. 36).
7. if the Hessian error $\|\Delta\tau - \mathcal{H}^{-1}y\|^2$ is too large, calculate the true Hessian, perform a line search, decrease trust region radius r .
8. force Hessian to satisfy second order conditions (Eq. 28), by changing the sign of the values that violate conditions.
9. update $\tau \rightarrow \tau + \Delta\tau$ and go back to 4.
10. update $\rho \rightarrow \rho + \tau^T \Delta\rho$, and go back to 1.

The trust region is used to obtain a more robust algorithm, is reset at each inner loop, it increases if things are going well, decreases if the iteration is having trouble, but it is kept between (r_{\min}, r_{\max}) , typically $(0.5, 3)$. We can keep track of $\tau, \nabla\tau$ computed, and restart the algorithm once in a while from the root of the 2D linear fit of $\nabla\psi(\tau)$.

We can easily extend this algorithm to two successive steepest descent-ascent directions, by performing a higher dimensional saddle-point optimization:

$$\min_{\alpha^{(n,n+1)}} \max_{\beta^{(n,n+1)}} \mathcal{L} \left(\rho + \tau^{(n+1)} \Delta\rho^{(n+1)} + \tau^{(n)} \Delta\rho^{(n)} \right)$$

The 4D optimization is performed using the same Newton/quasi-Newton trust-region optimization as in the 2D case.

A. Performance and conclusions

The algorithms were tested with a simple simulation. Fig. 4 was used to simulate a diffraction pattern, and several phase retrieval tests were performed using different random starts. When the error metric ε_m goes below a threshold that was seen as providing a good quality reconstruction it is stopped. Fig. 5 shows the relative performance of the various algorithms. By adding the 2D or 4D optimization the iterations converge more reliably and in less iterations to a solution (Table 1).

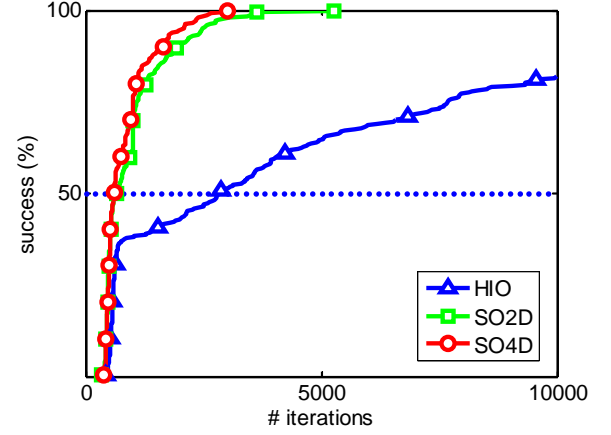


Fig. 5. Success rate, starting from random phases (250 trials).

Table 1. Benchmark of various algorithms (250 trials).

Algorithm	No. of iterations for		success rate (total)
	50% success	100% success	
HIO	2790	> 10000	82%
SO2D	656	5259	100%
SO4D	605	2999	100%

Acknowledgments

This work was performed under the auspices of the U.S. Department of Energy by the Lawrence Livermore National Laboratory under Contract No. W-7405-ENG-48 and the Director, Office of Energy Research. This work was partially funded by the National Science Foundation through the Center for Biophotonics, University of California, Davis, under Cooperative Agreement No. PHY0120999.

Appendix A: Two dimensional gradient and Hessian

The function \mathcal{L} in reciprocal space can be expressed as:

$$\begin{aligned} \mathcal{L}(\tilde{\rho}_s + \tilde{\rho}_{\underline{s}}) &= \left\| [I - \tilde{P}_m](\rho_s + \tilde{\rho}_{\underline{s}}) \right\|^2 - \left\| \tilde{\rho}_{\underline{s}} \right\|^2 \quad (\text{A1}) \\ &= \sum |\tilde{\rho}_s|^2 - 2\sqrt{I}|\tilde{\rho}_s + \tilde{\rho}_{\underline{s}}| + \sqrt{I} \end{aligned}$$

and the two components of the gradients:

$$\begin{aligned} \nabla\mathcal{L} &= 2 \begin{pmatrix} P_s \nabla\mathcal{L} \\ P_{\underline{s}} \nabla\mathcal{L} \end{pmatrix} = 2 \begin{pmatrix} P_s [I - P_m](\rho_s + \rho_{\underline{s}}) \\ -P_{\underline{s}} P_m(\rho_s + \rho_{\underline{s}}) \end{pmatrix} \quad (\text{A2}) \\ \nabla_s \mathcal{L} &= 2P_s [I - P_m](\rho_s + \rho_{\underline{s}}) \\ \nabla_{\underline{s}} \mathcal{L} &= -2P_{\underline{s}} P_m(\rho_s + \rho_{\underline{s}}) \end{aligned}$$

and corresponding steps $\Delta\rho_s = -\frac{1}{2}\nabla_s \mathcal{L}$, $\Delta\rho_{\underline{s}} = +\frac{1}{2}\nabla_{\underline{s}} \mathcal{L}$.

The function $\psi(\alpha, \beta)$ can be calculated in reciprocal space, provided that the components $\tilde{\rho}_{s,\underline{s}}, \Delta\tilde{\rho}_{s,\underline{s}}$ are

known:

$$\begin{aligned}
\psi(\alpha, \beta) &= \left\| [\mathbf{I} - \tilde{\mathbf{P}}_m] (\tilde{\rho} + \alpha \Delta \tilde{\rho}_s + \beta \Delta \tilde{\rho}_{\underline{s}}) \right\|^2 \\
&- \left\| \tilde{\rho}_{\underline{s}} + \beta \Delta \tilde{\rho}_{\underline{s}} \right\|^2 \\
&= \sum_{\mathbf{k}} \left\| \tilde{\rho} + \alpha \Delta \tilde{\rho}_s + \beta \Delta \tilde{\rho}_{\underline{s}} - \sqrt{I} \right\|^2 \\
&- \left\| \tilde{\rho}_{\underline{s}} + \beta \Delta \tilde{\rho}_{\underline{s}} \right\|^2 \\
&= \sum_{\mathbf{k}} I + |\tilde{\rho}_s + \alpha \Delta \tilde{\rho}_s|^2 \\
&- 2\sqrt{I} |\tilde{\rho} + \alpha \Delta \tilde{\rho}_s + \beta \Delta \tilde{\rho}_{\underline{s}}|
\end{aligned} \tag{A3}$$

Using common derivative rules:

$$\frac{\partial}{\partial x} |x| = \frac{x}{|x|}, \tag{A4}$$

$$\frac{\partial}{\partial \alpha} |x + \alpha \Delta x| = \frac{\Re(\Delta x^\dagger (x + \alpha \Delta x))}{|x + \alpha \Delta x|}, \tag{A5}$$

$$\frac{\partial}{\partial \alpha} \frac{x + \alpha \Delta x}{|x + \alpha \Delta x|} = \frac{\Delta x}{|x + \alpha \Delta x|} - \frac{x + \alpha \Delta x}{|x + \alpha \Delta x|^3} \cdot \frac{\Re(\Delta x^\dagger (x + \alpha \Delta x))}{|x + \alpha \Delta x|^2}, \tag{A6}$$

$$\frac{\partial}{\partial \alpha} |x + \alpha \Delta x|^2 = 2\Re(\Delta x^\dagger (x + \alpha \Delta x)), \tag{A7}$$

$$\frac{\partial^2}{\partial \alpha^2} |x + \alpha \Delta x| = \frac{|\Delta x|^2}{|x + \alpha \Delta x|} - \frac{\Re(\Delta x^\dagger (x + \alpha \Delta x))^2}{|x + \alpha \Delta x|^3}, \tag{A8}$$

$$\frac{\partial^2}{\partial \alpha^2} |x + \alpha \Delta x|^2 = |\Delta x|^2, \tag{A9}$$

and

$$\begin{aligned}
\frac{\partial^2 |x + \alpha \Delta x + \beta \Delta y|}{\partial \alpha \partial \beta} &= \frac{\Re(\Delta x^\dagger \Delta y)}{|x + \alpha \Delta x + \beta \Delta y|} \\
&- \frac{\Re(\Delta x^\dagger (x + \alpha \Delta x + \beta \Delta y))}{|x + \alpha \Delta x + \beta \Delta y|^3} \\
&\cdot \frac{\Re(\Delta y^\dagger (x + \alpha \Delta x + \beta \Delta y))}{|x + \alpha \Delta x + \beta \Delta y|^2},
\end{aligned} \tag{A10}$$

we can calculate the analytic expression for the gradient and Hessian.

The gradient components (writing $\tilde{\rho}_\tau = \tilde{\rho} + \boldsymbol{\tau}^T \boldsymbol{\Delta} \tilde{\rho} = \tilde{\rho} + \alpha \Delta \tilde{\rho}_s + \beta \Delta \tilde{\rho}_{\underline{s}}$) are:

$$\begin{aligned}
\nabla_t \psi &= 2 \langle \Delta \tilde{\rho} | [\tilde{\mathbf{P}}_s - \tilde{\mathbf{P}}_m] \tilde{\rho}_\tau \rangle_r, \\
\frac{\partial \psi}{\partial \alpha} &= 2 \langle \Delta \tilde{\rho}_s | [\mathbf{I} - \tilde{\mathbf{P}}_m] \tilde{\rho}_\tau \rangle_r, \\
\frac{\partial \psi}{\partial \beta} &= 2 \langle \Delta \tilde{\rho}_{\underline{s}} | [-\tilde{\mathbf{P}}_m] \tilde{\rho}_\tau \rangle_r,
\end{aligned} \tag{A11}$$

and the Hessian and starting from the simplest component:

$$\begin{aligned}
\frac{\partial^2 \psi}{\partial \beta^2} &= -2 \langle \Delta \tilde{\rho}_{\underline{s}} | \frac{\partial \tilde{\mathbf{P}}_m \tilde{\rho}_\tau}{\partial \beta} \rangle \\
&= 2 \sum -\frac{|\Delta \tilde{\rho}_{\underline{s}}|^2 \sqrt{I}}{|\tilde{\rho}_\tau|} + \frac{\Re(\Delta \tilde{\rho}_{\underline{s}}^\dagger \tilde{\rho}_\tau)^2 \sqrt{I}}{|\tilde{\rho}_\tau|^3} \\
&= 2 \sum -\frac{|\Delta \tilde{\rho}_{\underline{s}}|^2 \sqrt{I}}{|\tilde{\rho}_\tau|} + \frac{\sqrt{I}}{2|\tilde{\rho}_\tau|} \frac{\Re(\Delta \tilde{\rho}_{\underline{s}}^\dagger \tilde{\rho}_\tau)(\Delta \tilde{\rho}_{\underline{s}}^\dagger \tilde{\rho}_\tau + \Delta \tilde{\rho}_{\underline{s}} \tilde{\rho}_\tau^\dagger)}{|\tilde{\rho}_\tau|^2} \\
&= 2 \langle \Delta \tilde{\rho}_{\underline{s}} | -\frac{\sqrt{I}}{2|\tilde{\rho}_\tau|} \left(1 - \frac{\tilde{\rho}_\tau^2}{\Delta \tilde{\rho}_{\underline{s}}^2} \frac{|\Delta \tilde{\rho}_{\underline{s}}|^2}{|\tilde{\rho}_\tau|^2} \right) | \Delta \tilde{\rho}_{\underline{s}} \rangle_r
\end{aligned} \tag{A12}$$

$$\begin{aligned}
\frac{\partial^2 \psi}{\partial \alpha^2} &= 2 \langle \Delta \tilde{\rho}_s | \frac{\partial [\mathbf{I} - \tilde{\mathbf{P}}_m] \tilde{\rho}_\tau}{\partial \alpha} \rangle \\
&= 2 \sum |\Delta \tilde{\rho}_s|^2 - \frac{|\Delta \tilde{\rho}_s|^2 \sqrt{I}}{|\tilde{\rho}_\tau|} + \frac{\Re(\Delta \tilde{\rho}_s^\dagger \tilde{\rho}_\tau)^2 \sqrt{I}}{|\tilde{\rho}_\tau|^3} \\
&= 2 \langle \Delta \tilde{\rho}_s | \left[1 - \frac{\sqrt{I}}{2|\tilde{\rho}_\tau|} \left(1 - \frac{\tilde{\rho}_\tau^2}{\Delta \tilde{\rho}_s^2} \frac{|\Delta \tilde{\rho}_s|^2}{|\tilde{\rho}_\tau|^2} \right) \right] | \Delta \tilde{\rho}_s \rangle_r
\end{aligned} \tag{A13}$$

The cross terms:

$$\begin{aligned}
\frac{\partial^2 \psi}{\partial \beta \partial \alpha} &= 2 \langle \Delta \tilde{\rho}_s | \frac{\partial [\mathbf{I} - \tilde{\mathbf{P}}_m] \tilde{\rho}_\tau}{\partial \beta} \rangle \\
&= 2 \langle \Delta \tilde{\rho}_s | -\frac{\sqrt{I}}{2|\tilde{\rho}_\tau|} \left(1 - \frac{\tilde{\rho}_\tau^2}{\Delta \tilde{\rho}_{\underline{s}}^2} \frac{|\Delta \tilde{\rho}_{\underline{s}}|^2}{|\tilde{\rho}_\tau|^2} \right) | \Delta \tilde{\rho}_{\underline{s}} \rangle_r \\
&= 2 \langle \Delta \tilde{\rho}_{\underline{s}} | -\frac{\sqrt{I}}{2|\tilde{\rho}_\tau|} \left(1 - \frac{\tilde{\rho}_\tau^2}{\Delta \tilde{\rho}_s^2} \frac{|\Delta \tilde{\rho}_s|^2}{|\tilde{\rho}_\tau|^2} \right) | \Delta \tilde{\rho}_s \rangle_r
\end{aligned} \tag{A14}$$

The term () tends to 0 as $\Delta \tilde{\rho}_{\underline{s}}$ approaches $\tilde{\rho}_t$.

References

1. P. W. Hawkes & J. C. H. Spence (Eds.), *Science of Microscopy* (Springer, 2007).
2. J. R. Fienup, Opt. Lett. **3**, 27-29 (1978).
3. J. R. Fienup, Appl. Opt. **21**, 2758-2769 (1982).
4. A. Levi and H. Stark, J. Opt. Soc. Am. A **1**, 932-943 (1984).
5. H. Stark, *Image Recovery: Theory and applications* (Academic Press, 1987).
6. V. Elser, J. Opt. Soc. Am. A **20**, 40-55 (2003).
7. H. H. Bauschke, P. L. Combettes, and D. R. Luke, J. Opt. Soc. Am. A **19**, 1334-1345 (2002).
8. H. H. Bauschke, P. L. Combettes, and D. R. Luke, J. Opt. Soc. Am. A **20**, 1025-1034 (2003).
9. D. R. Luke, Inverse Problems **21**, 37-50 (2005), (arXiv:math.OA/0405208).
10. S. Marchesini, Rev. Sci. Instr. **77**, 1 (2006), (arXiv:physics/0603201).
11. D. R. Luke, J. V. Burke, R. G. Lyon, SIAM Review **44**, 169-224 (2002).
12. J. V. Burke and D. R. Luke, SIAM J. Control Opt. **42**, 576-595 (2003).
13. R. Gerchberg and W. Saxton, Optik **35**, 237-246 (1972).
14. W. H. Press, S. A. Teukolsky, W. T. Vetterling and B. P. Flannery, *Numerical Recipes in C* (Cambridge University Press, 1992).
15. M. R. Hestenes, *Conjugate Direction Methods in Optimization*, (Springer-Verlag, 1980).
16. R. Fletcher, *Practical Methods of Optimization* (John Wiley & Sons, 2000).
17. M. J. D. Powell, Lecture Notes in Mathematics **1066**, 122-141 (1984).
18. E. Polak, *Computational Methods in Optimization* (Academic Press, 1971).
19. J. Nocedal, S. J. Wright, *Numerical Optimization* (Springer Verlag, 2006).
20. J. R. Fienup, C. C. Wackerman, J. Opt. Soc. Am. A **3**, 1897-1907 (1986).

21. S. Marchesini, H. N. Chapman, A. Barty, M. R. Howells, J. C. H. Spence, C. Cui, U. Weierstall, and A. M. Minor, IPAP Conf. Series **7**, 380-382 (2006), (arXiv:physics/0510033).
22. J. Miao, C-C. Chen, C. Song, Y. Nishino, Y. Kohmura, T. Ishikawa, D. Ramunno-Johnson, T-K. Lee, and S. H. Risbud, Phys. Rev. Lett. **97**, 215503 (2006).
23. P.-T. Chen, M. A. Fiddy, C.-W. Liao and D. A. Pommet, J. Opt. Soc. Am. A **13**, 1524-31 (1996).
24. T. Isernia, G. Leone, R. Pierri, and F. Soldovieri, J. Opt. Soc. Am. A **16**, 1845-1856 (1999).
25. G. Oszlányi and A. Sütö, Acta Cryst. **A61**, 147-152 (2005).